J|A|C|S
ARTICLES
Published on Web 02/26/2002

Platinum Chalcogenido MCM-41 Analogues. High Hexagonal Order in Mesostructured Semiconductors Based on Pt^{2+} and $[Ge_4Q_{10}]^{4-}$ (Q = S, Se) and $[Sn_4Se_{10}]^{4-}$ Adamantane Clusters

Pantelis N. Trikalitis, Krishnaswamy K. Rangan, and Mercouri G. Kanatzidis*

Contribution from the Department of Chemistry, Michigan State University, East Lansing, Michigan 48824

Received October 5, 2001

Abstract: Highly periodic hexagonal honeycombs of platinum−germanium chalcogenide and platinum−tin selenide frameworks were prepared by linking corresponding $[Ge_4Q_{10}]^{4-}$ (Q = S, Se) and $[Sn_4Se_{10}]^{4-}$ clusters with Pt^{2+} ions. The non-oxidic honeycombs designated as C_nPyPtGeQ and C_nPyPtSnSe were templated by the lyotropic liquid-crystalline phase of alkylpyridinium surfactant $[C_nH_{2n+1}NC_5H_5]Br$ (C_nPyBr) with n= 12, 14, 16, 18, 20, and 22. Although the materials are amorphous at the microscale, they have crystalline mesoporosity with well-ordered and aligned surfactant-filled cylindrical pores. In addition to high mesoscopic order, the pore−pore separation is adjustable with the surfactant chain length (i.e., value of n). The quality of these materials, as judged by the degree of hexagonal order, rivals or exceeds that reported for the highest quality MCM-41 silicates. The materials have the lowest band gap reported so far for mesostructured chalcogenides solids, in the range $1.5 < E_g < 2.3$ eV. The C_nPyPtGeS analogues show intense photoluminescence at 77 K when excited with light above the band gap.

Introduction

The construction of solids with nanoscale features is the object of intense experimentation due to their anticipated useful technological applications.[1−6] Of particular interest have been open-framework solids with well-defined porosity in terms of shape and size.[7−14] The announcement in 1992 of a new family (MCM-X) of surfactant-templated silica mesoporous molecular sieves with regular pore shape and adjustable pore size sparked a fury of activity worldwide that resulted in an abundance of oxidic mesoporous solids with promising technological properties.[15−19] The use of long-chain organic liquid crystal templates to assemble inorganic structures is now a powerful synthetic tool in the synthesis of porous solids.[20,21,22] Whereas the mesoporous silicates and other oxides will impact for catalytic, separation, and adsorption applications, they lack interesting electronic or photonic properties. Bulk materials that combine mesoscale features and electronic properties are envisioned for novel applications in quantum electronics,[4,23−26] photonics,[27] and nonlinear optics,[28−30] among others. Such characteristics may be expected in non-oxidic materials such as the chalcogenides.[31−33] This has been the main impetus behind recent attempts by various groups to develop rational synthetic routes to such systems so they become readily available. The direct extension

(1) Hatzor, A.; Weiss, P. S. *Science* **2001**, *291*, 1019−1020.
(2) Huang, Y.; Duan, X. F.; Wei, Q. Q.; Lieber, C. M. *Science* **2001**, *291*, 630−633.
(3) Huczko, A. *Appl. Phys. A-Mater. Sci. Process.* **2000**, *70*, 365−376.
(4) Braun, P. V.; Osenar, P.; Stupp, S. I. *Nature* **1996**, *380*, 325−328.
(5) Ozin, G. A. *Adv. Mater.* **1992**, *4*, 612−649.
(6) Fendler, J. H. *Chem. Mater.* **1996**, *8*, 1616−1624.
(7) O'Keeffe, M.; Eddaoudi, M.; Li, H. L.; Reineke, T.; Yaghi, O. M. *J. Solid State Chem.* **2000**, *152*, 3−20.
(8) Zaworotko, M. J. *Angew. Chem., Int. Ed. Engl.* **2000**, *39*, 3052−3054.
(9) Rao, C. N. R. *Bull. Mater. Sci.* **1999**, *22*, 141−151.
(10) Yaghi, O. M.; Li, H. L.; Davis, C.; Richardson, D.; Groy, T. L. *Acc. Chem. Res.* **1998**, *31*, 474−484.
(11) Hue, Q. S.; Margolese, D. I.; Ciesla, U.; Feng, P. Y.; Gier, T. E.; Sieger, P.; Leon, R.; Petroff, P. M.; Schuth, F.; Stucky, G. D. *Nature* **1994**, *368*, 317−321.
(12) Hue, Q.; Leon, R.; Petroff, P. M.; Stucky, G. D. *Science* **1995**, *268*, 1324−1327.
(13) Cheetham, A. K.; Ferey, G.; Loiseau, T. *Angew. Chem., Int. Ed. Engl.* **1999**, *38*, 3269−3292.
(14) Barton, T. J.; Bull, L. M.; Klemperer, W. G.; Loy, D. A.; McEnaney, B.; Misono, M.; Monson, P. A.; Pez, G.; Scherer, G. W.; Vartuli, J. C.; Yaghi, O. M. *Chem. Mater.* **1999**, *11*, 2633−2656.
(15) Kresge, C. T.; Leonowicz, M. E.; Roth, W. J.; Vartuli, J. C.; Beck, J. S. *Nature* **1992**, *359*, 710−712.
(16) Beck, J. S.; Vartuli, J. C.; Roth, W. J.; Leonowicz, M. E.; Kresge, C. T.; Schmitt, K. D.; Chu, C. T. W.; Olson, D. H.; Sheppard, E. W.; McCullen, S. B.; Higgins, J. B.; Schlenker, J. L. *J. Am. Chem. Soc.* **1992**, *114*, 10 834−10 843.
(17) Sayari, A.; Liu, P. *Microporous Mater.* **1997**, *12*, 149−177.
(18) Corma, A. *Chem. Rev.* **1997**, *97*, 2373−2419.
(19) Ma, Y.; Tong, W.; Zhou, H.; Suib, S. L. *Microporous Mesoporous Mater.* **2000**, *37*, 243−252.
(20) Ying, J. Y.; Mehnert, C. P.; Wong, M. S. *Angew. Chem., Int. Ed. Engl.* **1999**, *38*, 56−77.
(21) Meier, W. *Curr. Opin. Colloid Interface Sci.* **1999**, *4*, 6−14.
(22) Schuth, F. *Chem. Mater.* **2001**, *13*, 3184−3195.
(23) Rajeshwar, K.; Tacconi, N. R.; Chenthamarakshan, C. R. *Chem. Mater.* **2001**.
(24) Sohn, L. L. *Nature* **1998**, *394*, 131−132.
(25) Sun, S. H.; Murray, C. B.; Weller, D.; Folks, L.; Moser, A. *Science* **2000**, *287*, 1989−1992.
(26) Murray, C. B.; Kagan, C. R.; Bawendi, M. G. *Science* **1995**, *270*, 1335−1338.
(27) Norris, D. J.; Vlasov, Y. A. *Adv. Mater.* **2001**, *13*, 371−376.
(28) Beecroft, L. L.; Ober, C. K. *Chem. Mater.* **1997**, *9*, 1302−1317.
(29) Ozin, G. A. *Supramol. Chem.* **1995**, *6*, 125.
(30) Ozin, G. A. In *Materials Chemistry*; American Chemical Society: Washington, DC, 1995; Vol. 245, pp 335−371.
(31) Li, H.; Eddaoudi, M.; O'Keeffe, M.; Yaghi, O. M. *Nature* **1999**, *402*, 276−279.
(32) Li, H. L.; Eddaoudi, M.; Laine, A.; O'Keeffe, M.; Yaghi, O. M. *J. Am. Chem. Soc.* **1999**, *121*, 6096−6097.
(33) Li, H. L.; Laine, A.; O'Keeffe, M.; Yaghi, O. M. *Science* **1999**, *283*, 1145−1147.

10.1021/ja017245b CCC: $22.00

of the synthetic method applied for the MCM-X family is not straightforward for non-oxides. For example, direct chalcogenide analogues to $[SiO_4]^{4-}$ units would be $[SiQ_4]^{4-}$ (Q = S, Se, Te), but such units are highly unstable to hydrolysis. The use of adamantane $[Ge_4Q_{10}]^{4-}$ anions has proven more useful in preparing mesostructured sulfide and selenide solids. These clusters are hydrolytically more stable and they can bind metal ions to form polymeric covalent chalcogenide frameworks. Ozin et al. reported the synthesis of hexagonal mesostructured solids by assembling adamantane $[Ge_4S_{10}]^{4-}$ units with metal ions (Ni^{2+}, Zn^{2+}, Co^{2+}, Cu_2^{2+}) in the presence of cationic surfactant molecules using formamide as a solvent.[34,35] Our group succeeded in synthesizing surfactant-templated semiconducting mesostructured materials based on discrete $[Ge_4Q_{10}]^{4-}$ (Q = S, Se) clusters and various linkage metal ions (Mn^{2+}, Zn^{2+}, Cd^{2+}, Hg^{2+}, Ga^{3+}, In^{3+}, Sb^{3+}, Sn^{4+}).[36−40] In the case of Ga^{3+}, In^{3+}, Zn^{2+}, and Sb^{3+} the resulting mesostructured systems photoluminesce strongly when excited and we have shown that the embedded surfactant C_nPy^+ molecules play a role.[39,40] The implications of this finding are that removal of the surfactant molecules in these systems may not always be sought, since some of the unique properties of these materials may derive *because* the surfactant species are still in the pores. The rational design and synthesis of semiconducting mesoporous framework solids was further enhanced by the use of the elementary tetrahedral Zintl anion $[SnSe_4]^{4-}$ and its binding to a variety of linkage metal ions. We showed that a cubic mesostructure (*Ia-3d*) is possible in the Cpy/Zn/$SnSe_4$ system.[41]

The type of chemistry used to construct these frameworks is fundamentally different from that used in the silicate system in which a self-polymerization of the $[SiO_4]^{4-}$ anions occurs. In contrast, the chalcogenido building units $[Ge_4Q_{10}]^{4-}$ (Q = S, Se) and $[SnSe_4]^{4-}$, which possess a tetrahedral topology, are linked together with the metal ions to form porous inorganic frameworks. The pores are occupied by the surfactant molecules, which are used as the structure-directing agent. It is often difficult to control the overall symmetry and organization of the pore system in these materials (i.e., wormhole, hexagonal, cubic, etc.) as each type is stabilized over a narrow set of experimental conditions. Outstanding issues as to how these systems form remain. For example, what role if any does the identity of the linkage metal ions play in achieving a given pore symmetry? Since the $[Ge_4Q_{10}]^{4-}/M^{n+}$ reactions are of the simple metathesis type, it is natural to ask, does ligand substitution kinetics and coordination preference of the metal play a role in controlling framework symmetry? If these issues are understood we may develop convenient synthetic routes to "tailor-made" materials with controlled pore symmetry under much broader, easier achievable sets of experimental conditions. Based on this rationale we explored the use of noble metals with strong and unique coordination preference, such as square planar Pt^{2+} ions, as linking cations in the construction of mesoporous chalcogenides. The results are both exciting and important as they lead to considerably improved order in the mesostructure and provide general new insights into the assembling process.

In this work we employed the clusters $[Ge_4Q_{10}]^{4-}$ (Q = S, Se) and $[Sn_4Se_{10}]^{4-}$ to construct surfactant templated frameworks with the noble Pt^{2+} ions. The alkylpyridinium bromides, C_nPyBr (n = 12, 14, 16, 18, 20, 22) where used as the surfactant templates. We demonstrate here for the first time that square planar Pt^{2+} ions by virtue of their relative kinetic inertness have a huge influence of the self-assembly reaction and give rise to the most well-ordered hexagonal mesostructured $[Ge_4Q_{10}]^{4-}$ (Q = S, Se) chalcogenides-based semiconductors known to date. It is also important to note that the introduction of noble metals in these frameworks is highly attractive because they could impart useful catalytic functionality in ways that may not be possible with the mesoporous silicates.[42] These materials are denoted as $C_nPyPtGeQ$ and $C_nPyPtSnSe$ where C_n signifies the length of the pyridinium surfactant chain. This also is the first report of the use of the $[Sn_4Se_{10}]^{4-}$ cluster as a band-gap modifying building block. The pore symmetry in these materials, as judged by the exceptional degree of hexagonal order, rivals or exceeds that of the highest quality MCM-41.[43]

Experimental Section

Starting Materials. $TMA_4[Ge_4S_{10}]$, $TMA_4[Ge_4Se_{10}]$ (TMA = tetramethylammonium), and $TEA_4[Sn_4Se_{10}]$ (TEA = tetraethylammonium) were synthesized in high yields (>90%) and pure form by a method developed in our laboratory.[44] K_2PtCl_4 was purchased from Strem Chemical Inc. Cetylpyridinium bromide monohydrate ($CPyBr{\cdot}H_2O$ or $C_{16}PyBr{\cdot}H_2O$) and formamide (FM) were purchased from Aldrich. The other surfactants were synthesized by reacting the corresponding alkyl bromide with excess pyridine in ethanol under reflux conditions. Pure compounds were obtained in high yield (>90%) after a single recrystallization from $CHCl_3$–ethyl acetate.

Mesostructured Platinum Germanium Sulfides C_nPyPtGeS. $TMA_4[Ge_4S_{10}]$ (0.907 g; 1 mmol) and alkylpyridinium bromide surfactant C_nPyBr (n = 12, 14, 16, 18, 20, 22) (4.0 g) were dissolved in 20 mL of FM at 80 °C forming a clear colorless solution. In a separate flask a solution of 1 mmol (0.415 g) of K_2PtCl_4 in 10 mL of FM was heated at 80 °C to form a red-orange solution and this was added to the surfactant/$[Ge_4S_{10}]$ solution over a period of 2 min by using a pipet. Interestingly, a yellow solid started to form after the first minute of the reaction and the mixture was aged overnight at 80 °C under stirring. The product was isolated by suction filtration, washed with copious amount of warm (80 °C) FM and H_2O, and dried under vacuum. Yield >80% based on $TMA_4[Ge_4S_{10}]$.

Mesostructured Platinum Germanium Selenide C_{16}PyPtGeSe. The reaction was carried out inside a glovebox under nitrogen. Cetylpyridinium bromide monohydrate (4.0 g) was dissolved in 20 mL of FM at 80 °C. In separate flasks 0.5 mmol (0.615 g) of $TMA_4[Ge_4Se_{10}]$ and 0.5 mmol (0.207 g) of K_2PtCl_4 dissolved in 10 mL of FM at 80 °C, forming clear dark orange and red solutions, respectively. These solutions were added simultaneously to the surfactant solution. A dark brown-red solid was formed within a few seconds and the mixture was

(34) MacLachlan, M. J.; Coombs, N.; Ozin, G. A. *Nature* **1999**, *397*, 681−684.
(35) MacLachlan, M. J.; Coombs, N.; Bedard, R. L.; White, S.; Thompson, L. K.; Ozin, G. A. *J. Am. Chem. Soc.* **1999**, *121*, 12 005−12 017.
(36) Rangan, K. K.; Billinge, S. J. L.; Petkov, V.; Heising, J.; Kanatzidis, M. G. *Chem. Mater.* **1999**, *11*, 2629−2632.
(37) Wachhold, M.; Rangan, K. K.; Lei, M.; Thorpe, M. F.; Billinge, S. J. L.; Petkov, V.; Heising, J.; Kanatzidis, M. G. *J. Solid State Chem.* **2000**, *152*, 21−36.
(38) Wachhold, M.; Rangan, K. K.; Billinge, S. J. L.; Petkov, V.; Heising, J.; Kanatzidis, M. G. *Adv. Mater.* **2000**, *12*, 85−91.
(39) Rangan, K. K.; Trikalitis, P. N.; Kanatzidis, M. G. *J. Am. Chem. Soc.* **2000**, *122*, 10230−10231.
(40) Rangan, K. K.; Trikalitis, P. N.; Bakas, T.; Kanatzidis, M. G. *Chem. Commun.* **2001**, 809−810.
(41) Trikalitis, P. N.; Rangan, K. K.; Bakas, T.; Kanatzidis, M. G. *Nature* **2001**, *410*, 671−675.
(42) The fuctionalization of mesostructured chalcogenides has not been pursued, however, we have made first steps in the direction with the synthesis of Fe_4S_4-MSU-*X* (*X* = 1, 2). *Angew. Chem., Int. Ed. Engl.* **2000**, *39*, 4558−4561
(43) Huo, Q. S.; Margolese, D. I.; Stucky, G. D. *Chem. Mater.* **1996**, *8*, 1147−1160.
(44) Novel convenient route to adamantane main group-chalcogenide molecular compounds. Trikalitis P. N.; Kanatzidis M. G., manuscript in preparation.

aged overnight at 80 °C under stirring. The product was isolated by suction filtration, washed with copious amount of warm (80 °C) FM and H_2O, and dried under vacuum. Yield >80% based on $TMA_4[Ge_4Se_{10}]$.

Mesostructured Platinum Tin Selenide C_{16}PyPtSnSe. The reaction was carried out inside a glovebox under nitrogen. Cetylpyridinium bromide monohydrate (4.0 g) was dissolved in 20 mL of FM at 80 °C. In separate flasks 0.39 mmol (0.7 g) of $TEA_4[Sn_4Se_{10}]$ and 0.39 mmol (0.163 g) of K_2PtCl_4 dissolved in 10 mL of FM at 80 °C forming dark orange and red solutions, respectively. These solutions were added simultaneously to the surfactant solution. A dark brown-red solid was formed within a few seconds and the mixture was aged overnight at 80 °C under stirring. The product was isolated by suction filtration, washed with copious amount of warm (80 °C) FM and H_2O, and dried under vacuum. Yield >80% based on $TEA_4[Sn_4Se_{10}]$.

Physical Measurements. Powder X-ray diffraction patterns were acquired on a Rigaku Rotaflex diffractometer (45 kV, 100 mA) using a rotating anode Cu Kα radiation source. The scan rates were between 0.10 and 0.15 deg/min and a step size of 0.01 deg. Quantitative microprobe analyses were performed on a JEOL JSM-6400V scanning electron microscope equipped with a Noran energy dispersive spectroscopy (EDS) detector. Data acquisition was performed with an accelerating voltage of 25 kV and 100-s accumulation time. Elemental C, H, N analyses were obtained on a Perkin-Elmer Series II CHNS/O Analyzer 2400. Pyrolysis mass spectra were obtained with a TRIO-1 mass spectrometer. Samples were heated at 20 °C/min and the volatile products were ionized by electron ionization.

Thermogravimetric analyses (TGA) were performed using a computer-controlled Shimadzu TGA-50 thermal analyzer. Typically, 40 mg of sample was placed in a silica bucket and heated in a nitrogen flow of 50 mL/min with a rate of 10 °C/min. Infrared spectra (IR) in the mid-IR region (4000−600 cm^{-1}, KBr pellet) and far-IR region (600−100 cm^{-1} CsI pellet) were recorded with a computer-controlled Nicolet 750 Magna-IR series II spectrometer equipped with a TGS/PE detector and silicon beam splitter in 2-cm^{-1} resolution. Raman spectra (3500−100 cm^{-1}) were recorded on a computer-controlled BIO-RAD Fourier transform FT-Raman spectrometer with a Spectra-Physics Topaz T10-106c 1064-nm YAG laser. The instrument was configured in 180° backscattering mode and the samples were loaded into melting point capillary tubes. UV/vis/near-IR diffuse reflectance spectra were obtained at room temperature on a Shimadzu UV-3101PC double-beam, double monochromator spectrophotometer in the wavelength range of 200−2500 nm. $BaSO_4$ powder was used as a reference (100% reflectance) and base material on which the powder sample was coated. Reflectance data were converted to absorbance data as described elsewhere.[45] Photoluminescence (PL) spectra were obtained on a Spex Fluorolog-2 F111AI spectrofluorimeter. Samples were loaded into 3 mm silica tubes and excitation and emission spectra were recorded at 77 K.

High-resolution transmission electron micrographs (TEM) were obtained with a JEOL 120CX instrument equipped with CeB_6 filament and operating at 120 kV. TEM samples were prepared by casting the powders on a holey carbon grid.

Results and Discussion

Synthesis. Mesostructured metal chalcogenides are typically assembled from two different precursors, an anion and a metal cation, via coordination reactions, in contrast to the oxides that normally form by the self-condensation polymerization process. The mesostructured sulfides reported to date are based primarily on $[Ge_4S_{10}]^{4-}$ cluster precursors and first-row transition and main-group ions such as Mn^{2+}, Co^{2+}, Ni^{2+}, Zn^{2+}, Cd^{2+}, In^{3+}, and Ga^{3+} whose coordination preference is mainly tetrahedral.[34−40] These cations are highly kinetically labile[46] so that, upon contact with the $[Ge_4S_{10}]^{4-}$ cluster in solution, they give rise to instantaneous precipitation of the product. This rapid process "freezes in" the inorganic framework, as dictated by the structure-directing organic surfactant, and as a consequence it irreversibly locks-in many disordered regions.

In this work we focused on slowing down the self-assembly reaction using a much less kinetically labile metal ion so that we allow the system more time to reach equilibrium, repairing possible defects, and achieve a more ordered (and presumably lower energy) structure. Further, the precise coordination geometry of Mn^{2+}, Co^{2+}, Ni^{2+}, Zn^{2+}, Cd^{2+}, In^{3+}, and Ga^{3+} in these complex materials is not known.[35,37,39] Although it is thought to be tetrahedral, higher coordination geometries such as five-coordinate or octahedral, and in the case of Ni^{2+} square planar, cannot be excluded. It is possible that the inorganic framework structure in these systems may be different from metal to metal. In this regard we chose the Pt^{2+} ion, because of its decidedly rigid square-planar coordination preference and its reduced kinetic lability in ligand substitution reactions, to explore the templated assembly of $[Ge_4Q_{10}]^{4-}$ and $[Sn_4Se_{10}]^{4-}$ cluster precursors according to

$$K_2PtCl_4 + TMA_4[Ge_4Q_{10}] + C_nPyBr \rightarrow C_nPyPtGeQ + TMA\text{-}Cl + KBr$$

Indeed, we find a striking difference in the behavior of the platinum systems with respect to that of the first-row transition and main-group ions. This reaction leads to a novel class of mesostructured materials with not only exceptional and unprecedented pore order but also catalytically interesting noble metal centers incorporated in the inorganic walls.

Our initial experiments using Pt^{2+} as the linkage metal were carried out using adamantane $[Ge_4S_{10}]^{4-}$ as the chalcogenido building block. Unlike in previous cases with other, kinetically labile linkage metals (Ni^{2+}, Zn^{2+}, Co^{2+}, Cu^{+}, Ga^{3+}, In^{3+}, Sb^{3+}, Sn^{4+}),[34,35,36−40] we observe a considerably slower reaction upon addition of the Pt^{2+} metal ions. That is, when the K_2PtCl_4/FM solution was added to the surfactant/$[Ge_4S_{10}]$ solution, instantaneous precipitation did not take place. The deposition of the mesophase began 1−1.5 min after and was complete in approximately 10−15 min. Similar behavior we observed in the case of $[Ge_4Se_{10}]^{4-}$ and $[Sn_4Se_{10}]^{4-}$; however, the reaction was much faster as compared to the surfactant/Pt/$[Ge_4S_{10}]^{4-}$ system. As we discuss below the platinum containing mesophases exhibit remarkably good hexagonal mesoscopic order. In contrast Pd^{2+} ions (which also possess strong square planar coordination preference), using K_2PdCl_4 as source, react much more rapidly, giving mesophases that do not exhibit notable high hexagonal order.[47]

The elemental composition of C_nPyPtGeQ (Q = S, Se) and C_nPyPtSnSe was determined with energy dispersive microprobe analysis (SEM/EDS), elemental C, H, N, and TGA analysis. A summary of analytical and other data is shown in Table 1. The results suggest a chemical formula $(C_nPy)_xPt_yM_4Q_{10+d}$ (M = Ge, Sn; Q = S, Se) with $1.9 < x < 2.8$ and $0.9 < y < 1.6$ for the mesophases (see Table 1). The germanium sulfide and selenide mesophases have a Pt:Ge_4 ratio higher than the value expected from the synthesis (1:4), especially the C_{20}PyPtGeS

(45) McCarthy, T. J.; Ngeyi, S. P.; Liao, J. H.; Degroot, D. C.; Hogan, T.; Kannewurf, C. R.; Kanatzidis, M. G. *Chem. Mater.* **1993**, *5*, 331−340.

(46) Atwood, J. D. *Inorganic and Organometallic Reaction Mechanisms*; BROOKS/COLE: Monterey, CA, 1985.

(47) Trikalitis, P. N.; Rangan, K. K.; Kanatzidis, M. G. *Mat. Res. Soc. Symp. Proc.* **2002**, *703*, in press.

Table 1. Summary of Elemental Analyses, Colors and Energy Band Gaps for the Mesostructured C_nPyPtGeS (n = 12, 14, 16, 18, 20, 22), C_{16}PyPtGeSe, and C_{16}PyPtSnSe Materials

mesophase	% C, H, N	TGA wt loss, %	Pt:M:Q[a]	formula[b]	color	band gap, eV
C_{12}PyPtGeS	28.79, 4.21, 2.40	39.2	1.2:4:11.4	$(C_{12}Py)_{1.9}Pt_{1.2}Ge_4S_{10.1}$	yellow	2.31
C_{14}PyPtGeS	33.29, 5.01, 2.13	44.1	1.3:4:11.9	$(C_{14}Py)_{2.1}Pt_{1.3}Ge_4S_{10.3}$	yellow	2.24
C_{16}PyPtGeS	40.42, 6.24, 2.14	48.6	1.1:4:11.2	$(C_{16}Py)_{2.6}Pt_{1.1}Ge_4S_{10.4}$	yellow	2.33
C_{18}PyPtGeS	38.77, 6.07, 2.04	48.4	1.2:4:12.2	$(C_{18}Py)_{2.3}Pt_{1.2}Ge_4S_{10.4}$	yellow	2.23
C_{20}PyPtGeS	41.57, 6.63, 2.04	51.1	1.5:4:12.6	$(C_{20}Py)_{2.6}Pt_{1.5}Ge_4S_{10.8}$	yellow	2.30
C_{22}PyPtGeS	44.49, 6.77, 1.98	54.2	1.6:4:12.9	$(C_{22}Py)_{2.8}Pt_{1.6}Ge_4S_{10.9}$	yellow	2.30
C_{16}PyPtGeSe	31.16, 4.97, 1.67	39.3	1.2:4:11.4	$(C_{16}Py)_{2.7}Pt_{1.2}Ge_4Se_{10.5}$	dark brown	1.81
C_{16}PyPtSnSe	30.14, 4.45, 1.62	35.7	0.9:4:11.9	$(C_{16}Py)_{2.7}Pt_{0.9}\ Sn_4Se_{10.3}$	dark brown	1.50

[a] EDS data normalized to four Ge atoms. [b] Combining all analytical data.

(1.5:4) and C_{22}PyPtGeS (1.6:4). Moreover, the ratio Ge:S is slightly lower than 4:10, indicating a possible excess of sulfur. These results can be explained if the clusters $[Ge_4S_{10}]^{4-}$ (when dissolved in formamide) are in equilibrium with other sulfide species, such as S^{2-} or $[Ge_2S_6]^{4-}$, originating from disproportionation of $[Ge_4S_{10}]^{4-}$ anions. Unfortunately, the lack of characteristic signature for S^{2-} makes it very difficult to detect by standard techniques (IR, Raman). Similar stoichiometries were reported previously for the $CTA_2M_2Ge_4S_{10}$ (M = Ni^{2+}, Zn^{2+}, Co^{2+}, Cu_2^{2+})[34,35] and CPMGeQ (Q = S, Se; M = Ga^{3+}, In^{3+}, Sb^{3+}, Sn^{4+})[39,40] mesophases as well as in the microporous TMA-CuGS-2 which contains a mixture of $[Ge_4S_{10}]^{4-}$ and S^{2-} anions.[48] Because higher than expected metal content and excess S^{2-} ions have now been observed in almost all cases involving $[Ge_4Q_{10}]^{4-}$ and formamide, it is tempting to speculate that these species are in fact *necessary* building blocks for the assembly of an ordered hexagonal framework. It is perhaps this reason that the degree of excess metal content varies with surfactant chain length C_n as a way for the framework to respond to the varying diameter of the micellar rods and changing charge matching requirements between cations and anions in the system.

Here it is fascinating to point out that electrostatic surfactant self-assembly of $M^{2+}/[Ge_4Q_{10}]^{4-}$ in water gave disordered wormhole type mesostructures[36−38] whose stoichiometry is more consistent with $(C_nTMA)_2MGe_4Q_{10}$ formula with no excess metal or sulfide ions. The facilitation of processes that result in Q^{2-} anions from $[Ge_4Q_{10}]^{4-}$ clusters in formamide and their total inhibition in water may explain why the formation of hexagonal structures in water is very difficult.[49]

X-ray Diffraction and Surfactant Chain Length. The mesostructured materials C_nPyPtGeQ and C_nPyPtSnSe show the sharpest most well-defined X-ray diffraction patterns known for any previously reported metal chalcogenide or even oxide mesophase and they are comparable to those reported for the highest quality MCM-41 system.[43,50,51] All samples show three or four well-defined Bragg reflections in the $2° < 2\theta < 7°$ region, characteristic of mesostructure material with regular hexagonal pore arrangement (see Figures 1 and 2). The remarkably intense, sharp, well-defined high order reflections

Table 2. Observed Bragg Reflections and Indexing for C_nPyPtGeS (n = 12, 14, 16, 18, 20, 22), C_{16}PyPtGeSe, and C_{16}PyPtSnSe Materials

mesophase	d_{100}, Å	d_{110}, Å	d_{200}, Å	d_{210}, Å	hexagonal unit cell constant, a_H,[a] Å
C_{12}PyPtGeS	27.4(7)				
C_{14}PyPtGeS	28.7(8)	16.8(9)	14.5(6)		33.6(3)
C_{16}PyPtGeS	34.5(1)	19.5(9)	16.9(9)	12.8(1)	39.2(2)
C_{18}PyPtGeS	34.1(1)	20.2(7)	17.7(1)	13.4(5)	40.8(1)
C_{20}PyPtGeS	36.6(6)	21.7(6)	18.9(6)	14.3(7)	43.6(9)
C_{22}PyPtGeS	40.7(1)	24.0(8)	20.8(4)	15.8(9)	48.2(6)
C_{16}PyPtGeSe	34.5(1)	19.9(9)	17.2(9)	12.9(8)	39.9(8)
C_{16}PyPtSnSe	35.7(7)	20.5(9)	18.1(5)		41.1(8)

[a] Refined based on all observed reflections using the program U_FIT. Evain, M. U_FIT: A cell parameter refinement program, I.M.N. Nantes (France), 1992.

(110) and (200), as well as the observation of the fourth (210) reflection, betray a high degree of hexagonal order in these systems as observed directly by transmission electron microscopy (TEM)(see below). The powder X-ray diffraction results along with peak indexing and lattice parameters for all materials are summarized in Table 2.

The effect of the surfactant chain length on the formation of the mesophases was investigated by using the series of surfactants $C_nPyBr{\cdot}xH_2O$ (n = 12, 14, 16, 18, 20, 22). The XRD patterns of C_nPyPtGeS samples[52] as a function of n are displayed in Figure 2. The patterns of C_nPyPtGeS for n = 16, 18, 20, and 22 show *four* sharp and intense low-angle reflections that define a hexagonal unit cell. For n = 14, three reflections, (100), (110), and (200), were observed, while for n = 12 the pattern shows only one broad low-angle peak corresponding to the (100) reflection. The degree of hexagonal order can be estimated from the relative intensities of the high order reflections (see Table 3). For example, the definition of the 4th order Bragg peak (210) becomes greater as n increases; see Figure 2. On this basis it is clear that with increasing surfactant chain length the long-range order of the hexagonal mesostructure increases substantially. The departure of the n = 12 member from the general trend suggests that when the surfactant chain becomes shorter than 14 carbon atoms long, favorable electrostatic or other interactions with the inorganic anions are no longer possible to permit hexagonal ordering.

The distance between the pore centers, represented by the unit cell constant (see Table 2 and Figure 3) monotonically increases with chain length in the range 33.6−48.2 Å. Figure 3 shows a nearly linear relationship between the hexagonal cell constant and the number of carbon atoms in the surfactant chain. A crude estimation of the wall thickness can be derived from

(48) Tan, K. M.; Ko, Y. H.; Parise, J. B.; Darovsky, A. *Chem. Mater.* **1996**, *8*, 448−53.
(49) Further support for the argument that formamide may promote cluster equilibria comes from speciation experiments in H_2O and formamide of $[Ge_4S_{10}]^{4-}$ and $[Sn_4Se_{10}]^{4-}$ solutions involving mass spectrometry and NMR spectroscopy. These indicate that the behavior in the two solvents is dramatically different. The results of these experiments we have done will be reported later.
(50) Edler, K. J.; White, J. W. *Chem. Mater.* **1997**, *9*, 1226−1233.
(51) Edler, K. J.; Reynolds, P. A.; White, J. W.; Cookson, D. *J. Chem. Soc., Faraday Trans.* **1997**, *93*, 199−202.

(52) We observed similar behavior in the systems C_nPyPtGeSe and C_nPyPtSnSe, n = 12, 14, 18, 20, and 22. The results will be pubslished elsewhere.

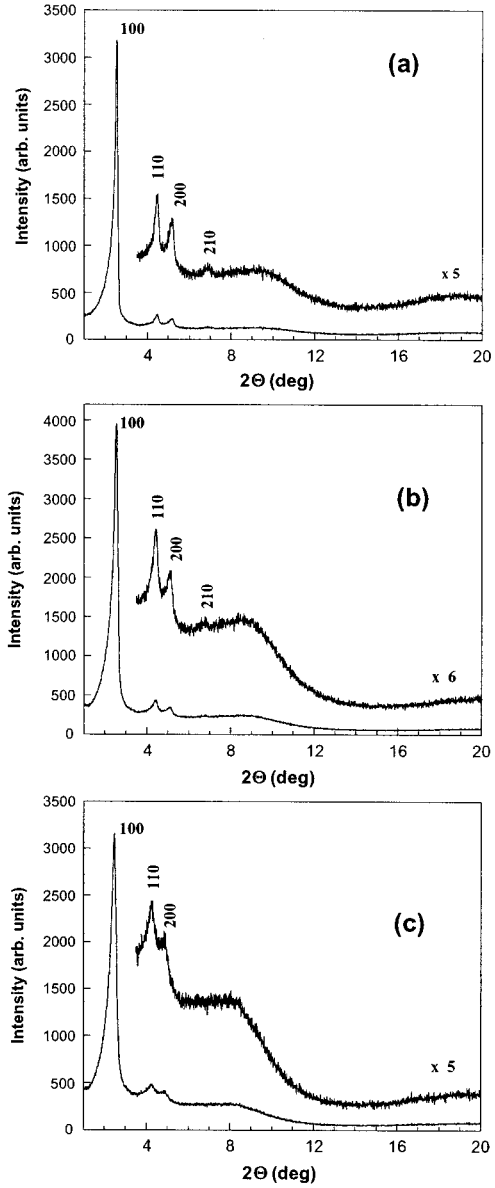

Figure 1. X-ray diffraction patterns of mesostructured platinum chalcogenides: (a) C_{16}PyPtGeS, (b) C_{16}PyPtGeSe, and (c) C_{16}PyPtSnSe (Cu Kα radiation).

the intercept of the linear equation (i.e., extrapolating to $n = 0$), which gives approximately 11 Å. For comparison, a typical wall thickness for MCM-41 materials is also about 10 Å.[53] The monotonic increase of the pore−pore separation and the apparent greater matching of the organic/inorganic parts of the structure for hexagonal symmetry with increasing n suggest that the inorganic framework may also have to be adjusting its composition and local atom connectivity in response to increasing micellar cylinder size. Therefore the local arrangement of building blocks in C_nPyPtGeS may vary with n. An indication of this comes from the increased Pt content in the structure when the long-chain surfactants C_{20}PyBr and C_{22}PyBr are used (see Table 1).

Undoubtedly the surfactant system C_nPyBr increasingly favors the formation of high-quality hexagonal mesophases with growing n. In contrast, in the case of MCM-41 silica, the mesostructural order *decreases* when long chain alkyltrimethylammonium surfactant is used ($n = 18, 20, 20$).[43,54−56] Similarly, in the mesostructured $[CTA]_2M_2Ge_4S_{10}$ ($M = Ni^{2+}$, Zn^{2+}, Co^{2+}, Cu_2^{2+}) materials,[34,35] the best hexagonal order is observed in the system CTA-Ni/Ge_4S_{10}, which, however, is less ordered compared to the platinum mesophases reported here. The use of longer surfactant chain in this case, C_{18}TMA-Ni/Ge_4S_{10}, gave a less ordered hexagonal phase along with a lamellar phase as impurity.

Again the relative intensities of the (110) and (200) reflections in the XRD patterns can be used to assess the degree of order in these materials and to compare with the so-called high-quality hexagonal MCM-41 silica.[16,43,50,51] The high pore symmetry and the domain size of the honeycombs in these materials are reflected in the XRD patterns with an increase in the relative intensities of the high-order reflections (110), (200), and (210). Table 3 displays the normalized intensities of all observed Bragg reflections, including those from a conventional, Mobil MCM-41 sample[15,16] and a representative "high-quality" MCM-41 sample.[43] The relative intensities of the (110) and (200) reflections in the latter case and in the case of C_nPyPtGeQ and C_nPyPtSnSe are comparable and considerably stronger than those of the Mobil variety (see Table 3). Therefore, it is apparent that the mesostructured platinum chalcogenides reported here are of similar structural quality to the best MCM-41 systems. An exception in Table 3 is C_{12}PyPtGeS, which gave one broad low-angle peak at 28 Å.

A final point we wish to make is that the pore order in C_{16}Py-Zn/Ge_4S_{10}[34,35] and C_{16}Py-M/Ge_4Q_{10} ($M = Ga^{3+}$, In^{3+}, Sb^{3+}, Sn^{4+})[39,40] mesophases is inferior to those reported here. This underscores the significant role of square-planar Pt^{2+} as the linkage metal to produce high-quality hexagonal mesostructured phases in this system. Ozin et al. suggested that the Ni in the system CTA-Ni/Ge_4S_{10} was not present in a tetrahedral environment but more likely in a square-planar geometry.[35] Perhaps then it is not a coincidence that the system CTA-Ni/Ge_4S_{10} showed the highest hexagonal symmetry out of the entire group of surfactant/M/Ge_4S_{10}, $M = Ni^{2+}$, Zn^{2+}, Co^{2+}, Cu_2^{2+}. The results reported here support this proposal.

Transmission Electron Microscopy (TEM). Samples of the mesostructured C_nPyPtGeQ and C_nPyPtSnSe were examined by TEM. Because the materials were environmentally stable, no particular sample preparation was necessary other than some gentle grinding. The samples were stable under the electron beam during the experiment. A large survey of the samples showed that all the particles possessed mesoscopic order. No dense phases were evident and very little amorphous material was observed. Interestingly, single particles of C_nPyPtGeQ and C_nPyPtSnSe did not show worm-shaped morphologies as observed in CTA-M/Ge_4S_{10}[34,35] and MCM-41.[15,16] Figure 4a,b shows characteristic images of C_{16}PyPtGeSe and C_{16}PyPtSnSe looking down the pore channel axis ([100] direction) where a remarkably uniform and extensive hexagonal order is clearly visible. Figures 4c,d show a view of C_{16}PyPtGeSe and C_{16}PyPtSnSe perpendicular to the pore axis ([110] direction). The long, straight parallel tunnels are apparent in these images and the observed interpore distances are in good agreement with

(53) Kruk, M.; Jaroniec, M.; Sayari, A. *Chem. Mater.* **1999**, *11*, 492−500.
(54) Kruk, M.; Jaroniec, M.; Sakamoto, Y.; Terasaki, O.; Ryoo, R.; Ko, C. H. *J. Phys. Chem. B* **2000**, *104*, 292−301.
(55) Ryoo, R.; Ko, C. H.; Park, I. S. *Chem. Commun.* **1999**, 1413−1414.
(56) Sayari, A.; Yang, Y. *J. Phys. Chem. B* **2000**, *104*, 4835−4839.

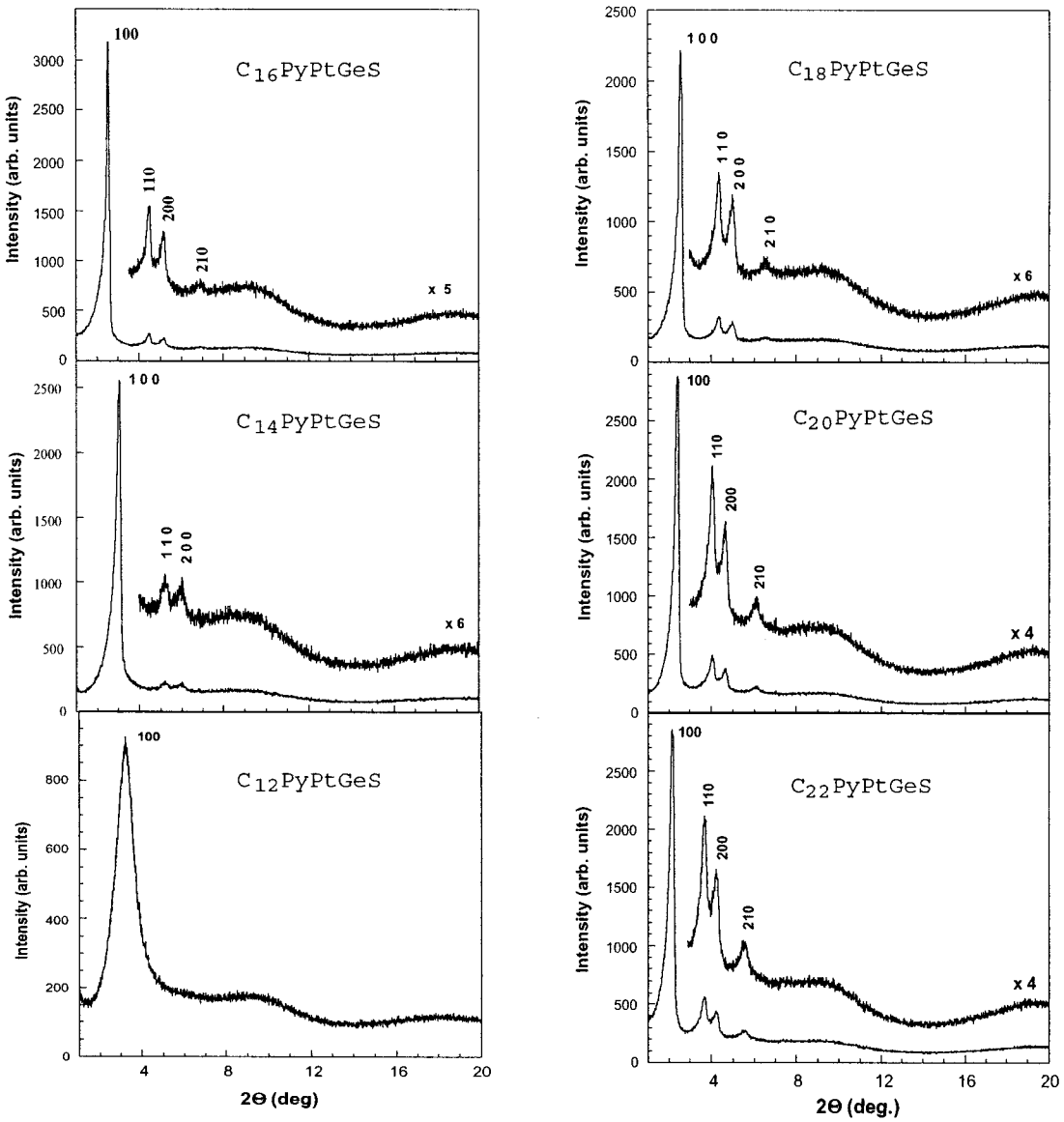

Figure 2. X-ray powder diffraction patterns of mesostructured C_nPyPtGeS where $n = 12$, 14, 16, 18, 20, and 22 (Cu Kα radiation). When $n = 12$ full hexagonal order is not achieved.

Table 3. Comparison of Experimental Relative X-ray *hkl* Intensities[a] of C_nPyPtGeQ, C_{16}PyPtSnSe Materials, and "Conventional" and "High Quality" MCM-41 Samples

hkl	C_{14}PyPtGeS	C_{16}PyPtGeS	C_{18}PyPtGeS	C_{20}PyPtGeS	C_{22}PyPtGeS	C_{16}PyPtGeSe	C_{16}PyPtSnSe	Mobil MCM-41[b]	high-quality MCM-41[c]
100	100	100	100	100	100	100	100	100	100
110	3.7	5.1	8.6	12.2	14.4	5.9	7.4	1.8	13.4
200	3.5	3.6	6.7	8.0	9.9	3.5	5.2	1.6	6.9
210		1.0	1.5	2.5	3.7	0.8a		0.2	1.3

[a] Normalized to 100 for the strongest *hkl* peak. [b] Conventional sample from ref 15, 16. [c] From ref 43.

those obtained from the X-ray diffraction patterns (Table 2). Figure 5 shows a TEM image of a large C_{16}PyPtGeSe particle where the size of coherent, hexagonally organized domain is >500 nm. In fact the honeycomb motif was observed to pervade the full body of particles as large as 1 μm. The optical diffraction pattern of this image (inset) demonstrates the good crystalline quality of the pores by displaying several *hk*0 reflections.

Infrared and Raman Spectroscopy. Infrared (IR) and Raman spectroscopy was used to examine the inorganic framework and also to confirm the presence of the surfactant molecules in these materials. In the mid-IR region we observed the characteristic absorption bands of alkylpyridinium cations. Shown in Figure 6 are typical far-IR spectra from C_{16}PyPtGeS, C_{16}PyPtGeSe, and C_{16}PyPtSnSe samples, together with the corresponding spectra from the free adamantane clusters for comparison (see also Table 4). In all cases the spectra show characteristic peaks in the same range as the free adamantane clusters, but they are much broader, indicating possible different bonding environments present.

FT-Raman spectra were collected for the mesostructured C_nPyPtGeS materials, while for the C_{16}PyPtGeSe and C_{16}PyPtSnSe spectra could not be obtained as they decomposed under

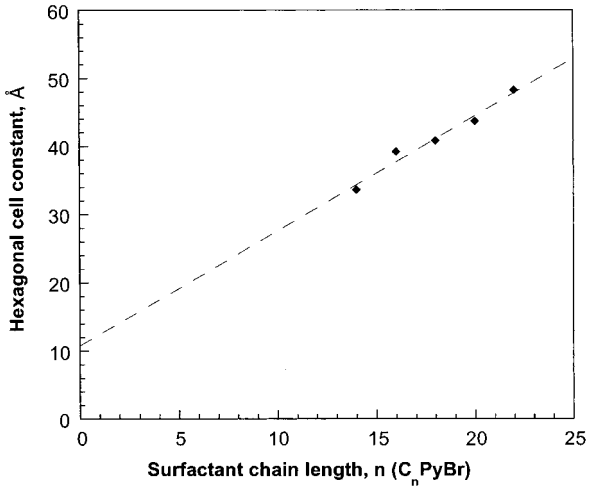

Figure 3. Variation in the hexagonal cell constant of the C_nPyPtGeS materials with the number of carbon atoms in the aliphatic chain of the surfactant used.

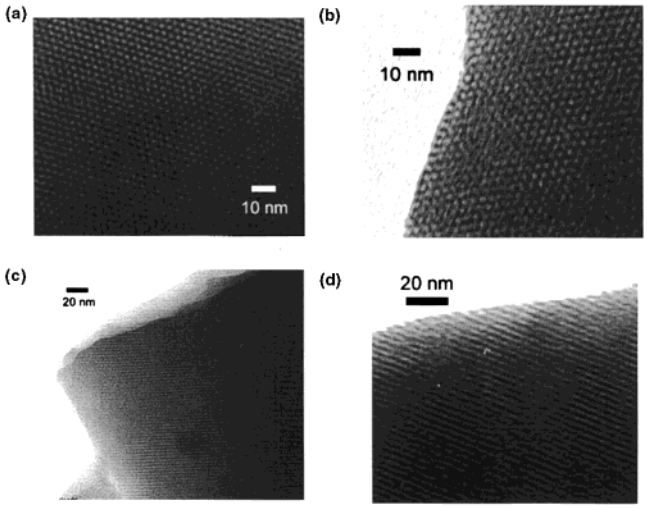

Figure 4. TEM images of mesostructured chalcogenides: (a) C_{16}PyPtGeSe looking down the pore channel axis; (b) C_{16}PyPtSnSe looking down the pore channel axis; (c) C_{16}PyPtGeSe view perpendicular to the channel axis; (d) C_{16}PyPtSnSe view perpendicular to the channel axis.

the laser beam. Figure 7 shows typical spectra from the C_nPyPtGeS materials in the far-Raman region (600−100 cm^{-1}) were several vibrational modes attributed to Ge−S and Pt−S stretching modes are observed. From a comparison with previous Raman studies in compounds containing metal-linked adamantane $[Ge_4S_{10}]^{4-}$ clusters,[35,57] the sharp peak centered at 376 cm^{-1} can be assigned to the totally symmetric breathing mode of the "Ge_4S_6" cage, while the peak at 440 cm^{-1} is assigned to the terminal Ge−S_t stretching mode. The peak at 340 cm^{-1} can be assigned to the Pt−S vibration, according to the spectroscopic analysis of Raman spectrum of PtS.[58]

Thermal Stability. The mesostructured C_nPyPtGeQ and C_nPyPtSnSe are markedly stable over time. Samples that had been hydrothermally posttreated at 100 °C over 2 days showed XRD patterns that were virtually identical to those of as-prepared samples. The thermal stability of the mesostructured solids was

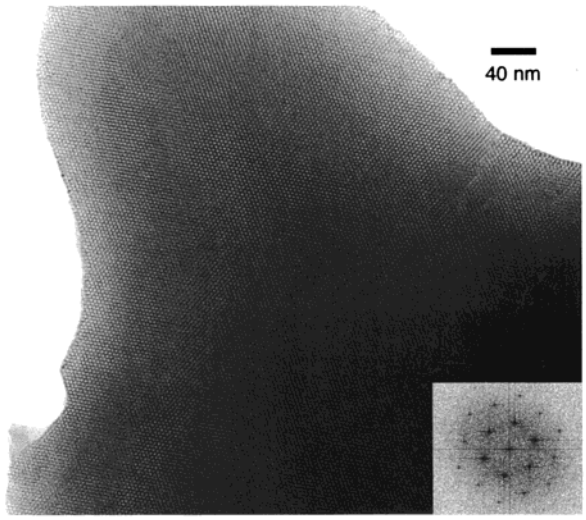

Figure 5. Representative image of a large particle of C_{16}PyPtGeSe showing the hexagonal organization extending over its full body. Particle length >500 nm. The insert at lower right is an optical Fourier transform of the image showing well-defined hexagonal spots in reciprocal space.

investigated with thermogravimetric analysis (TGA) and pyrolysis mass spectrometry (MS). Shown in Figure 8 are characteristic TGA curves of C_{16}PyPtGeS, C_{16}PyPtGeSe, and C_{16}PyPtSnSe. The compounds show no appreciable weight loss up to 190 °C, consistent with the fact that they contain no solvent molecules. Between 190 and 450 °C, weight loss occurs in a two-step process due to surfactant decomposition, and this is evident from the slope change occurring at ∼290 °C in the TGA curves of C_{16}PyPtGeSe and C_{16}PyPtSnSe, see Figure 8. In the cases of C_nPyPtGeS and C_{16}PyPtGeSe, the inorganic residue at 600 °C is amorphous platinum germanium sulfide or selenide, while in the case of C_{16}PyPtSnSe crystalline $SnSe_2$ also formed.

Pyrolysis mass spectrometry at 250 °C of the released volatiles shows a strong peak with *m*/*z* 79, which corresponds to the pyridyl headgroup of the surfactant, the first species to leave the solid. On further heating, $C_nH_{2n+1}S^+$ or $C_nH_{2n+1}Se^+$ were detected, showing that the platinum chalcogenide framework is attacked during this process. The detection of $C_nH_{2n+1}S^+$ or $C_nH_{2n+1}Se^+$ is strong evidence that the collapse of the mesostructure occurs by a chemical transformation and not a physical one as suggested previously for the mesoscopic CTA-M/Ge_4S_{10}.[35] This makes sense since the surfactant molecules are positively charged and must undergo some form of neutralization, which in this case includes attack of the framework during heating. Formally, for every two surfactant molecules lost, a chalcogen atom has to be removed from the inorganic walls. This changes the framework composition too dramatically to sustain structural integrity. Whereas the silica walls of MCM-41 can replace framework oxygen loss from water or air and are able to undergo condensation−polymerization of residual hydroxyls, heal, and reconstruct to maintain the integrity of the structure, the metal−chalcogenide framework cannot. Therefore to remove the surfactant molecules and access the pore space in these materials, new mechanisms of removal must be sought and developed. Nevertheless, here we wish to emphasize that surfactant removal may not be necessary, or desirable, to exploit the properties of these systems. Many electronic and photonic processes may be displayed or achieved *because* the surfactant species are in fact present. Particularly

(57) MacLachlan, M. J.; Scott, R. W. J.; Ozin, G. A.; McIntosh, D. F. *J. Chem. Educ.* **2000**, *77*, 630−632.
(58) Pikl, R.; De Waal, D.; Merkle, R. K. W.; Verryn, S. M. C. *Appl. Spectrosc.* **1999**, *53*, 927−930.

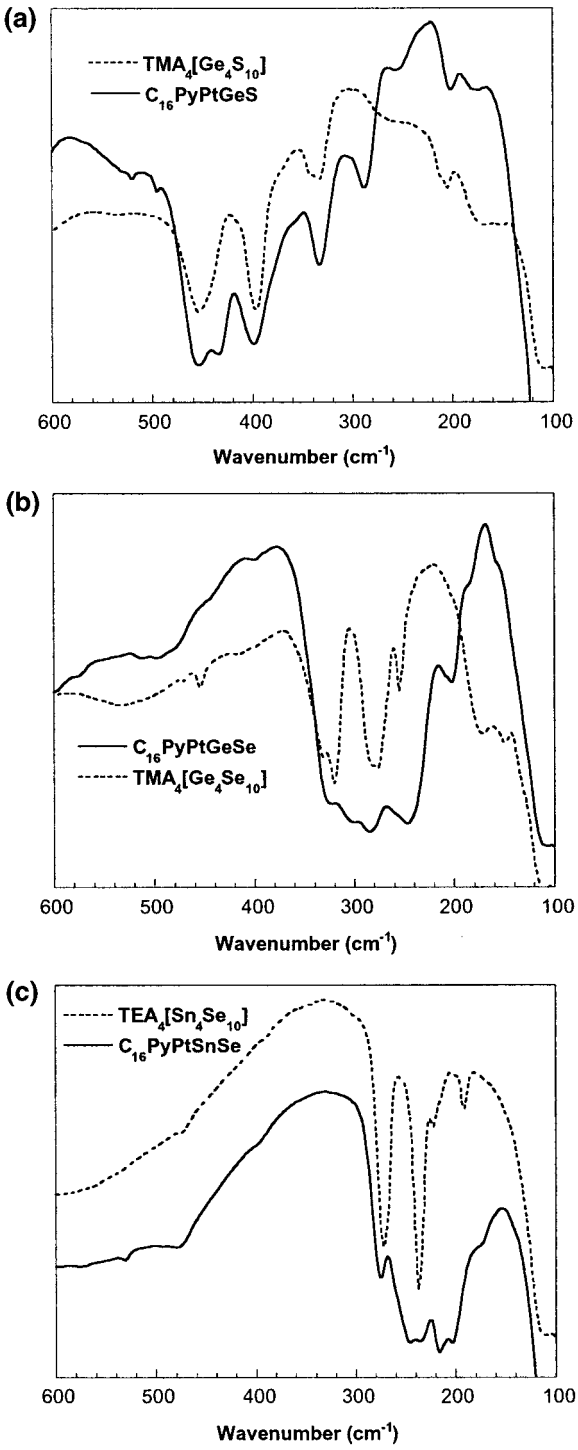

Figure 6. Far-IR spectra (CsI pellets) of (a) $C_{16}PyPtGeS-TMA_4[Ge_4S_{10}]$, (b) $C_{16}PyPtGeSe-TMA_4[Ge_4Se_{10}]$, and (c) $C_{16}PyPtSnSe-TEA_4[Sn_4Se_{10}]$.

interesting is the prospect of novel properties that derive from strong physicochemical interactions between the organic and inorganic parts of the structure. In this regard mesoscopic metal chalcogenide semiconductors should be investigated with specially designed surfactants possessing interesting functional groups. The prospect of a useful role for the surfactant molecules of mesostructured silica and other materials (where the general rule is to remove the organic part before any further investigation) has began to be increasingly recognized.[22,62] Indeed novel properties were discovered for the as-synthesized (surfactant included) mesostructured silica solids.[59−62]

Table 4. Far-Infrared Absorptions (cm^{-1}) for $C_{16}PyPtGeS$, $C_{16}PyPtGeSe$, $C_{16}PyPtSnSe$, and Corresponding Precursor Adamantane Molecular Salt Compounds

$C_{16}PyPtGeS$	$TMA_4[Ge_4S_{10}]$	$C_{16}PyPtGeSe$	$TMA_4[Ge_4Se_{10}]$	$C_{16}PyPtSnSe$	$TEA_4[Sn_4Se_{10}]$
178 (m, sh)	170 (m)	182 (m, sh)	149 (m)	174 (m, sh)	190 (s)
201 (m)	205 (m)	201 (s)	172 (m)	202 (s)	222 (s)
252 (m)	267 (m,sh)	246 (vs)	254 (s)	215 (s)	236 (vs)
287 (vs)	337 (s)	286 (vs)	279 (vs)	234 (s)	271 (vs)
333 (vs)	396 (vs)	301 (s)	319 (vs)	245 (s)	
399 (vs)	454 (vs)	326 (vs)	332 (s)	275 (vs)	
435 (s)			454 (m)		
455 (vs)					

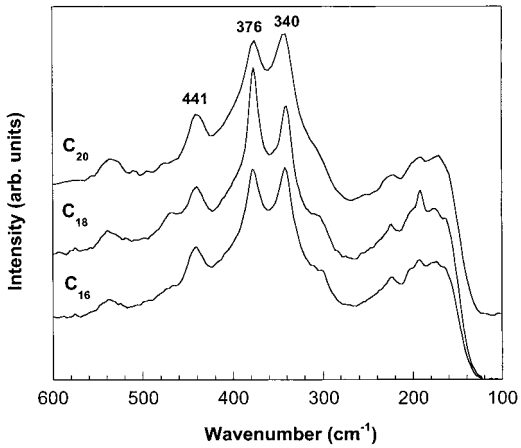

Figure 7. Raman spectra of $C_nPyPtGeS$ (n = 16, 18, 20).

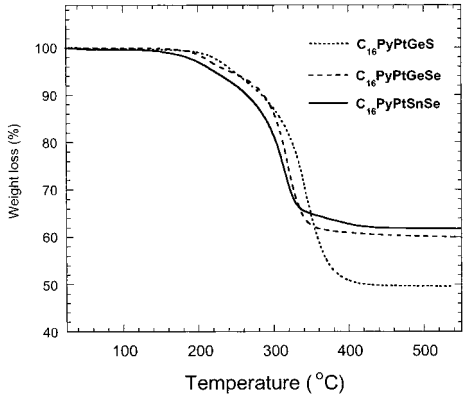

Figure 8. TGA curves of $C_{16}PyPtGeS$, $C_{16}PyPtGeSe$, and $C_{16}PyPtSnSe$ under nitrogen flow (heating rate 10 deg/min).

Optical Properties. The optical absorption properties of the $C_nPyPtGeQ$ and $C_nPyPtSnSe$ mesostructured solids were investigated with solid-state diffuse reflectance UV−vis/near-IR spectroscopy. All solids possess well-defined, sharp optical absorptions associated with band gap transitions in the energy range 2.3−1.5 eV (see Table 1 and Figure 9a,b). The adsorption edge of the $C_nPyPtGeS$ (n = 12, 14, 16, 18, 20, 22) materials is independent of the surfactant chain length and occurs at ∼2.3 eV, Figure 9a. The band gap narrows in going from the lighter, $C_{16}PyPtGeS$, to the heavier, $C_{16}PyPtGeSe$ (1.8 eV) and $C_{16}PyPtSnSe$ (1.5 eV), analogues (see Figure 9b and Table 1). Moreover, the effect on the band gap in going from the $[Ge_4S_{10}]^{4-}$ to $[Ge_4Se_{10}]^{4-}$ based frameworks is much greater

(59) Wu, J.; Abu-Omar, M. M.; Tolbert, S. H. *Nanoletters* **2001**, *1*, 27−31.
(60) Wu, J. J.; Liu, X. Y.; Tolbert, S. H. *J. Phys. Chem. B* **2000**, *104*, 11837−11841.
(61) Kubota, Y.; Nishizaki, Y.; Sugi, Y. *Chem. Lett.* **2000**, 998−999.
(62) Sayari, A.; Hamoudi, A. *Chem. Mater.* **2001**.

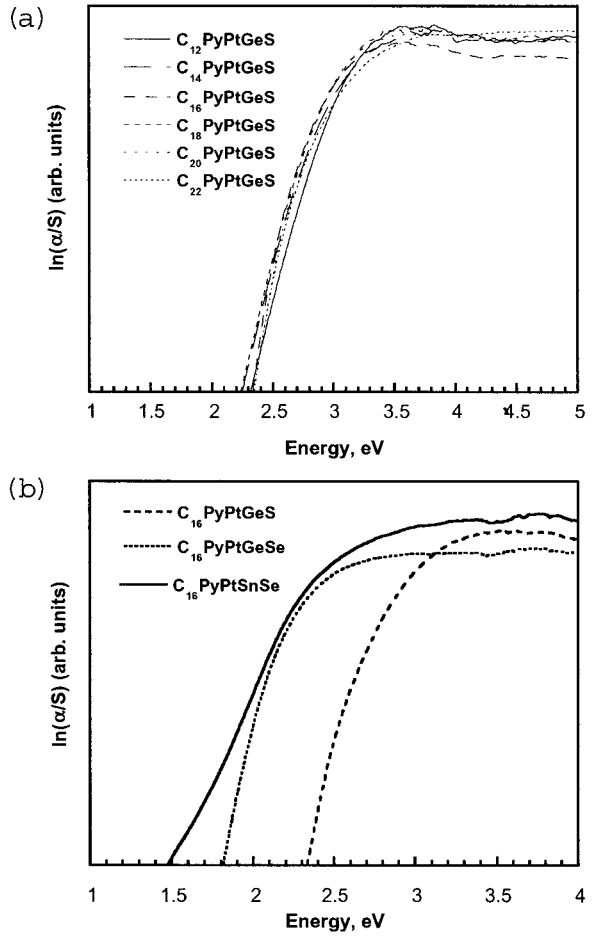

Figure 9. Solid-state UV−vis absorption spectra of $C_nPyPtGeQ$ and $C_nPyPtSnSe$ materials.

than in going from $[Ge_4Se_{10}]^{4-}$ to $[Sn_4Se_{10}]^{4-}$, suggesting a more dominant role of the chalcogenide element in the valence and conduction band of the materials.

The band gaps reported here are the lowest among the mesostructured chalcogenide solids reported so far.[34,35,36−40] In addition, for a given adamantane building block, $[Ge_4Q_{10}]^{4-}$, the use of Pt^{2+} as the linkage metal, compared with other metals used (e.g., Zn^{2+}, Cd^{2+}, Hg^{2+}, Ga^{3+}, In^{3+}, Sb^{3+}, Sn^{4+}), clearly narrows the band gap. For example, the sulfide members of the mesostructured $[C_nH_{2n+1}NMe_3]M^{II}Ge_4Q_{10}$ (M^{II} = Zn^{2+}, Cd^{2+}, Hg^{2+} and Q = S, Se)[37] show band gaps between 3.2 and 3.4 eV, while the corresponding selenide phases have values from 2.3 to 2.6 eV. Apparently, the optical absorption properties in these solids are framework dependent and can be tuned in a consistent manner.

Light Emission. The mesostructured platinum germanium sulfide materials, $C_nPyPtGeS$, showed intense photoluminescence (PL) when excited with light above the band gap. (Figure 10). With an excitation line at 2.61 eV (476 nm) the materials show intense red-pink emission at 77 K, with two closely spaced maxima at 1.79 eV (693 nm) and 1.85 eV (671 nm). Recently we have shown in the systems CPMGeS (M = Ga, In)[39] and CPSbGeS[40] that the PL involves both the pyridinium chromophore of the surfactant and the inorganic framework. Each component alone is not capable of producing the observed response in these systems. To probe if this were also the case for the PL response of the $C_nPyPtGeS$ systems, we prepared

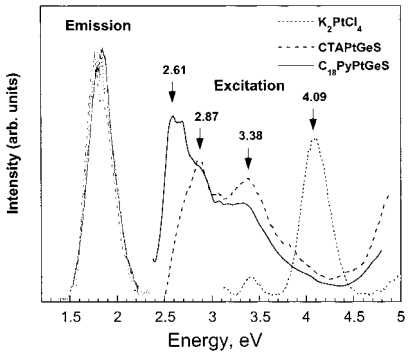

Figure 10. Photoluminescence and excitation spectra of K_2PtCl_4 (dotted line), CTAPtGeS (dashed line), and $C_{18}PyPtGeS$ (solid line) (77 K).

hexagonal mesostructured CTAPtGeS (CTA: cetyltrimethylammonium) where the CTA cation does not luminesce.[63] Remarkably, the CTAPtGeS shows PL at 77 K (see Figure 10). The excitation spectrum detected at 1.77 eV (701 nm) shows two maxima at 2.87 eV (432 nm) and 3.38 eV (367 nm). With an excitation line at 2.87 eV (432 nm), intense red-pink emission was observed with two closely spaced maxima at 1.77 eV (701 nm) and 1. 84 eV (675 nm), very similar to the emission spectra of the $C_nPyPtGeS$ materials. The same emission spectrum was observed with an excitation line at 3.38 eV (367 nm). This indicates clearly that the PL of the $C_nPyPtGeS$ materials originates from the inorganic framework, in contrast to other metal−germanium sulfide mesophases[39,40] in which the absence of chromophore in the surfactant eliminates the PL.

To elucidate the origin of the PL in $C_nPyPtGeS$, the photoluminescence and excitation spectrum of K_2PtCl_4 was recorded at 77 K (see Figure 10). The luminescence properties of square-planar Pt^{2+} compounds are known and have been well-documented in the past.[64−69] With an excitation line at 4.09 eV (303 nm), intense red-pink emission centered 1.80 eV (690 nm) was observed, in agreement with previous reports,[64] with almost the same energy as the emission from $C_nPyPtGeS$ (see Figure 10). Undoubtedly, the PL property of the $C_nPyPtGeS$ originates from the square-planar Pt^{2+} centers.

Conclusions

High hexagonal mesopore symmetry is not limited to MCM-41 silicas. The use of square-planar Pt^{2+} ions in a supramolecular assembly of adamantane $[Ge_4Q_{10}]^{4-}$ and $[Sn_4Se_{10}]^{4-}$ clusters leads to a new class of non-oxide mesostructured materials with exceptionally high hexagonal symmetry. The preferred square-planar geometry of the platinum and the slower reaction kinetics[46,70] of framework assembly seem to be deciding factors for the formation of high-quality, extended hexagonal mesophases in the system surfactant/metal/M_4Q_{10} (M = Ge, Sn; Q

(63) The full chemistry and properties of these related systems are under investigation.
(64) Webb, D. L.; Ancarani Rossiello, L. *Inorg. Chem.* **1970**, *9*, 2622−2625.
(65) Viaene, L.; Ceulemans, A.; Vanquickenborne, L. G. *Inorg. Chem.* **1985**, *24*, 1713−1716.
(66) Preston, D. M.; Guntner, W.; Lechner, A.; Gliemann, G.; Zink, J. I. *J. Am. Chem. Soc.* **1988**, *110*, 5628−5633.
(67) Sacksteder, L.; Baralt, E.; Degraff, B. A.; Lukehart, C. M.; Demas, J. N. *Inorg. Chem.* **1991**, *30*, 2468−2476.
(68) Reber, C.; Zink, J. I. *J. Phys. Chem.* **1991**, *95*, 9151−9158.
(69) Nelson, J. H.; Wilson, W. L.; Cary, L. W.; Alcock, N. W.; Clase, H. J.; Jas, G. S.; RamseyTassin, L.; Kenney, J. W. *Inorg. Chem.* **1996**, *35*, 883−892.
(70) Schmuelling, M.; Ryabov, A. D.; Van Eldik, R. *J. Chem. Soc., Chem. Commun.* **1992**, 1609−1611.

= S, Se). The materials show regular pore expansion with increasing surfactant chain length from C_{12} up to C_{22}. Moreover, the degree of the hexagonal order rises in these systems with increasing the chain length, underscoring the significant role of the alkylpyridinium surfactant as a template. C_nPyPtGeQ and C_nPyPtSnSe possess optical band gaps, ranging between $1.5 < E_g < 2.3$ eV, in the desirable region for optical applications. The band gap narrows with the incorporation of heavier elements in the framework. The C_nPyPtGeS materials emit light when excited with light above the band gap at 77 K, an emission that originates from the amorphous inorganic framework and especially from the Pt^{2+} ions. The C_{16}PyPtSnSe represents the first example of mesostructured solid prepared from the adamantane unit $[Sn_4Se_{10}]^{4-}$ and exhibits the lowest optical band gap (1.5 eV).[71] These results clearly point to the systematic control of framework properties.

Unlike the highly flexible silicate units, the building blocks, (Pt^{2+} and $[M_4O_{10}]^{4-}$ clusters) that combine to assemble a three-dimensional ordered structure, can be regarded as well defined, rigid objects. In this context, understanding framework assembly and structure in these systems may be easier than in silicas. Thus they can serve as model systems to help achieve a more fundamental understanding of the interplay between kinetic and thermodynamic factors and how they control structure assembly in these complex materials.

Acknowledgment. The support of this research by NSF-CRG Grant CHE 99-03706 is gratefully acknowledged. This work made use of the SEM and TEM facilities of the Center of Advanced Microscopy at MSU.

JA017245B

(71) We have prepared also crystalline microporous solids based on $[Sn_4Se_{10}]^{4-}$ and transition metals. Trikalitis P. N.; Kanatzidis M. G., manuscript in preparation.